Light-induced switching to a Metastable Phase in a Layered Superconductor $La_{2-x}Sr_xCuO_4$ (x=0.15)

Kaito Tomari[1], Ryusuke Matsunaga[1,2,3], Hiroaki Niwa[1], Dongjoon Song[4], Hiroshi Eisaki[4], and Ryo Shimano[1,5]

[1]*Department of Physics, The University of Tokyo, Hongo, Tokyo, 113-0033, Japan*

[2]*PRESTO, Japan Science and Technology Agency, 4-1-8 Honcho Kawaguchi, Saitama 332-0012, Japan*

[3]*Laser and Synchrotron Research Center, The Institute for Solid State Physics, The University of Tokyo, 5-1-5 Kashiwanoha, Kashiwa, Chiba, 277-8581, Japan*

[4]*National Institute of Advanced Industrial Science and Technology, Tsukuba 305-8568, Japan*

[5]*Cryogenic Research Center, The University of Tokyo, Yayoi, Tokyo, 113-0032, Japan*

Abstract

We investigated transient optical responses in an optimally-doped high-T_c superconductor $La_{2-x}Sr_xCuO_4$ (x=0.15) by using 800-nm optical pump and terahertz probe spectroscopy. With increasing the photoexcitation intensities, the Josephson plasma resonance shows a gradual redshift, indicating the suppression of superconductivity by the photoexcitation. With further increasing the photoexcitation intensities, a new longitudinal mode in the loss function spectrum appears and grows from the high energy side, accompanied by a new transverse mode as manifested in the conductivity spectrum. The observed spectra are described by the multilayer model with alternating interlayer Josephson couplings. The new longitudinal and transverse modes sustain much longer than several hundred picoseconds after the photoexcitation, indicating that the new metastable phase with possessing alternating interlayer Josephson couplings is induced by the strong photoexcitation.

In unconventional high-temperature superconductors (SC), it has been revealed that various electronic states emerge depending on temperature and chemical doping, such as antiferromagnetic insulator, spin density wave, stripe order, charge order, pair density wave, nematic order, and pseudogap [1]. It is now commonly recognized that the elucidation of the competition or mutual couplings of those multiple orders as well as the unveiling of pairing glue is crucial to understand the emergence of superconductivity. In these aspects, the study of real-time dynamics of superconductivity by ultrafast spectroscopy technique has been playing important roles. For instance, ultrafast pump-probe experiments have shown its ability to elucidate bosonic fluctuations to which fermionic quasiparticles couple [2-4]. Time-resolved observation of collective modes enables the direct access to the order parameter dynamics in nonequilibrium [5, 6], and for cuprate SCs it has been used to reveal the coupling between the superconductivity and the charge density wave order [7, 8]. Searching for a new state of matter induced by the photoexcitation is also a fascinating subject in this respect, as it provides deeper insight into the competing orders or hidden states, with revealing new functionalities of correlated materials. Light-induced superconductivity is a striking example, which has been investigated *e.g.* by photodoping to the parent compound [9], and recently by strongly pumping the phonon modes in the mid-infrared range [10, 11], or by suppressing the competing stripe charge order by near infrared pumping [12-14]. In particular, in the latter two cases, the experiments have shown the appearance of Josephson plasma resonance (JPR) above the critical temperature (T_c) [10-14], indicating that the superconducting-like state is induced although the phenomena last only several ps after the photoexcitation. Extensive theoretical studies have since been devoted to account for the light-induced superconductivity, while the mechanism remains under strong debates. The role of intense photoexcitation remains to be elucidated, even in the doping region where a signature of competing orders is obscured.

In this Letter, we investigated the photoexcited dynamics in optimally-doped $La_{2-x}Sr_xCuO_4$ (x=0.15) (LSCO) where no static stripe order exists, by using near-infrared optical-pump and THz-probe spectroscopy. In the weak excitation regime, the superconductivity is gradually suppressed with increasing photoexcitation densities,

as manifested by the continuous redshift of the JPR. However, when the photoexcitation intensity exceeds ~1 mJ/cm^2, a new metastable phase emerges characterized by the appearance of new longitudinal and transverse JPRs.

Figure 1(a) shows a schematic of our optical pump-THz probe experiment. We used a single crystalline optimally-doped LSCO with T_c=35.5 K. The mirror-polished *ac* surface of the sample (7×7×5 mm^3) is used and masked by a metal plate with a tapered 4-mm hole. A gold mirror is also mounted on the sample holder as a reference of reflectance. We used a Ti:Sapphire-based amplified laser with pulse energy of 4.2 mJ, repetition rate of 1 kHz, pulse duration of 100 fs, and center wavelength of 800 nm. The output of the laser is divided into three beams: for the optical pump, the generation of the THz probe, and the gate pulse for the THz time-domain spectroscopy, respectively. The THz pulse is generated by the optical rectification in a large-area ZnTe crystal and linearly polarized along the *c* axis of LSCO. The reflected THz pulse is detected by the electro-optic sampling in a ZnTe crystal with the gate pulse. The optical pump beam has a Gaussian profile with $1/e^2$ diameter of 9 mm, which ensures spatial uniformity of excitation density on the probed region.

Figure 1(b) shows the temperature dependence of reflectivity spectra in equilibrium without pump, showing a clear plasma edge below T_c. As temperature decreases the plasma edge shows a blueshift and approaches to 7.6 meV, indicating the development of bulk superconductivity. The loss function Im[-1/$\varepsilon(\omega)$] and the real-part optical conductivity $\sigma_1(\omega)$ are shown in Figs. 1(c) and (d), respectively. The loss function spectrum exhibits a single peak corresponding to the longitudinal JPR, while $\sigma_1(\omega)$ is featureless indicating the absence of transverse mode. These spectral profiles in equilibrium agree well with previous studies [15-18].

Next we investigate the transient response at 5 K under the optical pump linearly polarized along the *c*-axis. We also investigated the pump polarization along the *a* axis and obtained similar results (See Supplemental Material [19]). We fixed the gate pulse delay at the peak of the probe THz waveform and scanned the pump-probe delay *t*. Figure 2(b) shows the pump-induced change of the peak electric field, $\delta E_{\mathrm{probe}}$, as a

function of t for various excitation intensities. After the instantaneous changes within the time resolution (~1 ps) of the THz probe pulse, the signal decays with the time constant of ~40 ps, subsequently followed by a much long-lived component. The lifetime of this long-lived state is longer than our scan range of several hundred picoseconds. A slight kink discerned at 20 ps is an artifact caused by the multiple reflections of the pump pulse along the optical path.

Figure 2(c) shows the raw data of transient reflectivity for various pump intensities I_{pump} at a fixed delay of t=100 ps where the system is considered to reach a quasistatic state. The plasma edge shows a redshift for I_{pump}<<1 mJ/cm^2, implying the photoinduced suppression of superconductivity. Strikingly, when the pump intensity is further increased, another plasma edge appears from the higher-frequency side. Figure 2(d) shows the transient reflectivity spectra for various delays t with I_{pump}=3.6 mJ/cm^2. The new plasma edge is most prominent at t=3 ps, and gradually attenuates with t but robustly sustains even at t=350 ps. At the negative delay time, t=-5 ps, a slight redshift of the plasma edge is discerned, which is attributed to the heating of the sample due to the laser irradiation. The amount of temperature rise in the negative delay is evaluated as ~5 K from the comparison with the spectrum without the pump, which does not affect following discussions.

To analyze the data further, we must take into account the difference of penetration depth between the pump and probe pulses: the penetration depth of the optical pump is estimated as 600 nm from the literatures [16, 19], whereas the THz probe penetrates more deeply than the pump. To extract the response function of the photoexcited surface region, we assume that the refractive index at the distance z from the surface is given by

$$n(\omega, z) = n_{\mathrm{eq}}(\omega) + \left[n(\omega) - n_{\mathrm{eq}}(\omega)\right]\exp\left(-z / d_{\mathrm{pump}}\right), \qquad (1)$$

where $n(\omega)$ and $n_{\mathrm{eq}}(\omega)$ are the refractive indices of the photoexcited surface region and of equilibrium without pump, respectively [10, 12]. Then we decompose the photoexcited region into a series of thin layers and extract $n(\omega)$.

First we consider the case of low excitation intensity regime, I_{pump}<0.5 mJ/cm^2,

where only a continuous redshift of the plasma edge is observed in the raw reflectivity spectra (Fig. 2(c)) with increasing the pump intensities. We fix the value of d_{pump} to the penetration depth, 600 nm. The obtained reflectivity, Im[-1/$\varepsilon(\omega)$], $\sigma_1(\omega)$, and $\sigma_2(\omega)$ spectra of the photoexcited surface regions are summarized in Figs. 3(a)-3(d). As I_{pump} increases, the plasma edge and loss function peak show a continuous redshift and no more identified at 470 μJ/cm^2. This result indicates that the *c*-axis superconducting coherence is destroyed upon the photoexcitation.

Here we compare the excitation density with previous studies in terms of the suppression of superconductivity. Ultrafast dynamics of the photoexcited LSCO has been studied by transient reflectivity measurements at 800 nm [20, 21] and by THz transmittance measurements [21]. In the thin-film experiment in nearly optimal-doped LSCO (x=0.16) [21], the absorbed energy density required to destroy the superconductivity at t=100 ps after the photoexcitation, where the electronic system and the lattice system are considered to reach quasithermal equilibrium, was evaluated as 13.7 K/Cu from the saturation behavior of the pump-probe signal. The photoexcitation intensity that corresponds to 13.7 K/Cu in our experiment is estimated as I_{pump}~150 μJ/cm^2. This value is consistent with the results shown in Fig. 3(a)-3(d) that JPR remains to exist at I_{pump}=48 μJ/cm^2 while it disappears at I_{pump}=470 μJ/cm^2.

Next, we consider the strong excitation regime, I_{pump}>0.5 mJ/cm^2. It should be noted here that if we use a fixed value of 600 nm for d_{pump} in the analysis of such a strong photoexcitation regime, the obtained response functions of the photoexcited surface region become unphysical [19]. This is because d_{pump} in Eq. (1) does not exactly correspond to the pump penetration depth but rather corresponds to the length scale where the system is influenced by the pump. Having seen that the pump-induced change of the response function is significant already at I_{pump}=48 μJ/cm^2 in Figs. 3(a)-3(d), d_{pump} should be extended longer than 600 nm for much stronger excitations. Therefore, we have to treat d_{pump} as a pump intensity-dependent value for the strong excitation [19]. First we examined various values of d_{pump} and extracted the response functions for each excitation density. Then we focused on the low-frequency behavior of the imaginary-part conductivity, $\sigma_2(\omega)$. $\sigma_2(\omega)$ should be extrapolated to 0 in the dc limit

(ω=0) in the normal state, while for the superconducting state$\sigma_2(\omega)$ diverges toward ω=0. Since JPR disappears already at I_{pump}=470 μJ/cm^2, it is reasonable to take the values of d_{pump} so that $\sigma_2(\omega)$ asymptotically approaches to 0 at ω=0 in the stronger excitation regime. In this way we obtained the response functions of the photoexcited surface region as shown in Figs. 3(e)-3(h). The values of d_{pump} are also shown in Fig. 4(a). In the Supplemental Material [19] we examined the validity of the value of d_{pump}, and confirmed that, in fact, the prominent spectral features in Figs. 3(e)-3(h) are less sensitive to the values of d_{pump}.

Strikingly, Figs. 3(e)-3(h) show that, after the loss function spectrum becomes featureless at I_{pump}=470 μJ/cm^2, another longitudinal mode appears at high-frequency side in the stronger excitation densities. In addition, a transverse mode appears as a sharp peak in $\sigma_1(\omega)$. In Fig. 4(b), we plot the peak energies of the loss function (circles) and conductivity (square) as a function of the pump intensity. Such an emergence of the *c*-axis transverse mode reminds us the response of *T**-type or bilayer cuprate SCs, *e.g.*, $SmLa_{1-x}Sr_xCuO_{4-\delta}$ [22-25], $YBa_2Cu_3O_{7-\delta}$ (YBCO) [12, 26], or $Bi_2Sr_2CaCu_2O_z$ [27]. For example, in a bilayer system, nonequivalent inter- and intra-bilayer Josephson couplings give rise to two distinct longitudinal resonances and one transverse optical mode. The emergence of transverse plasma modes has also been reported in YBCO under the presence of static magnetic fields where the Josephson vortices alternately modulate the interbilayer coupling [28, 29]. It is also noteworthy that recently the JPR-like double longitudinal modes have been reported to appear in the transient response of under-doped YBCO above T_c shortly after the strong excitation of apical oxygen phonon mode at 15 μm [13].

From the similarity of the obtained spectra with those of the bilayer system or Josephson vortex phases, it is likely that the strong photoexcitation induces an alternating modification of the interlayer Josephson couplings, although LSCO is a single layer cuprate SC. Therefore, to account for the observed results, we applied the multilayer model [30, 31] which has been formulated to describe the *c*-axis response of layered cuprate SCs with two distinct Josephson couplings. According to the multilayer

model, the local dielectric function for each coupling is described as $\varepsilon_j(\omega) = \varepsilon_\infty\left[1 - \omega_j^2/\omega^2 + i\Gamma_j/\omega\right]$ (j=A, B), where ε_∞ is the background dielectric constant, ω_j and Γ_j are the local coupling energy and the quasiparticle damping at the junction j. The overall response function is then given by

$$\varepsilon(\omega) = \left[\sum_j \frac{z_j}{\varepsilon_j(\omega)}\right]^{-1}, \qquad (2)$$

where z_A and z_B(=1-z_A) represent weight factors which include the effect of finite electron compressibility to incorporate plasma dispersion [31]. With this model, we performed numerical fits to the reflectivity, Im[-1/$\varepsilon(\omega)$], $\sigma_1(\omega)$, and $\sigma_2(\omega)$ spectra of the surface region, respectively, in particular for the high excitation densities, as represented in Figs. 3(i)-3(l). The used parameters are shown in Supplemental Material [19]. The experimental results are reasonably well reproduced, except for the intermediate excitation density of 470-1100 μJ/cm^2 which we discuss later, suggesting the emergence of two distinct interlayer Josephson couplings upon the strong photoexcitation. The calculated curves for the pump intensities below 48 μJ/cm^2 in Figs. 3(i)-3(l) are obtained from the fits to the experimental data by using a single layer model with the reduced JPR.

We can identify that JPR is gradually reduced and no more identified above 470 μJ/cm^2, which means that the 3-dimensional superconductivity is destroyed. By contrast, a new peak in Im[-1/$\varepsilon(\omega)$] and also in $\sigma_1(\omega)$ grow above 1100 μJ/cm^2, indicating that a local Josephson coupling devolps under strong photoexcitation. This photoinduced metastable phase can be thought of a bilayer-like state where the intra-bilayer superconducting coherence exists without 3-dimensional coherence, as schematically shown in Fig. 4(c). In fact, such a behavior resembles that of a bilayer SC YBCO in equilibrium where the onset of transverse plasma mode reaches 180 K in the strongly underdoped samples indicating the growth of intra-bilayer coupling without inter-bilayer coherence far above T_c =58 K [32].

Now we discuss mechanisms for the photoinduced metastable multilayer phase. One possibility is that the photoexcitation onto the *ac* surface induces vortex-antivortex

pair creations into the block layers, which would act like a superlattice of Josephson vortices with periodically modulating the interlayer coupling. But it seems difficult to explain how the photoexcitation induces magnetic fluxes penetrating deeply into the bulk region without breaking the time-reversal symmetry. Another scenario is that the interlayer distance is modulated due to the strong photoexcitaton. In an oxygen-doped parent material $La_2CuO_{4+\delta}$, it has been reported from ultrafast electron diffraction measurements that the strong laser irradiation at 800 nm induces an increase of the *c*-axis lattice constant and results in a structural phase transition above the fluence of 5 mJ/cm^2 [33]. Such a structural phase transition may also occur in LSCO, and indeed a previous optical pump-probe study in $La_{1.9}Sr_{0.1}CuO_4$ has reported that a qualitative change in the pump-probe signal sets in at 5 mJ/cm^2 [34]. Since this value is substantially larger than the photoexcitation density where the metastable phase starts to appear, ~0.5 mJ/cm^2, in our experiment, this picture is not sufficient to account for the emergence of the alternating Josephson couplings. Yet, it is worth noting that the local superconducting-like state is identified at I_{pump}=3.6 mJ/cm^2 even though the photoexcitation intensities far exceeds the superconducting condensation energy. This result suggests that a substantial energy injected by the photoexcitation goes to the lattice system. A closer look into the spectra in Figs. 1(d) and 3(c) shows that a broad absorption band appears in $\sigma_1(\omega)$ spectra around 10 meV which becomes most prominent at I_{pump}=470-1100 μJ/cm^2 and reduces at higher excitation densities. The origin of this band is not clear at moment, while it may be related to the one which has been previously reported in the equilibrium spectrum of $\sigma_1(\omega)$ at slightly lower frequencies, 4-6 meV, for the Sr-doping of around x=1/8 [15, 17, 35-37]. Importantly, the photoinduced transverse JPR mode seems distinct from this broad absorption band around 10 meV, as it starts to appear around 1100 μJ/cm^2 as a tiny peak on top of this broad absorption band with a much sharper resonance width. To elucidate the mechanism for the alternating modulation of the Josephson coupling in the *c*-axis direction, however, further comprehensive studies are needed, *e.g.* by time-resolved Raman, X-ray or electron diffraction with systematically changing the Sr-doping in LSCO.

In summary, we investigated the effect of strong photoexcitation at 800 nm in an

optimally doped LSCO where no static stripe order exists. We found a photo-switching phenomenon from superconducting to a metastable phase as characterized by the emergence of new longitudinal and transverse plasma modes, which sustains at least in the order of nanoseconds. The multilayer model analysis well reproduces the experimental results, suggesting that the photoinduced phase consists of a combination of Josephson-coupled layers and the disconnected layers. While the elucidation of microscopic mechanism for the emergence of such a metastable ordered phase requires further experimental and theoretical studies, our experimental observation may suggest the instability of the interlayer Josephson coupling against a fluctuation that results in the alternating modulation. The results would also provide a new insight into the photoexcited nonequilibrium phenomena in layered high-T_c cuprate SCs, as well as in its equilibrium.

We thank Y. Gallais and S. Uchida for fruitful discussions. This work was supported in part by JSPS KAKENHI (Grants Nos. JP15H02102, JP26247057, and JP15H05452), by the Photon Frontier Network Program from MEXT, Japan, and by JST PRESTO (Grants No. JPMJPR16PA).

Figure captions

Fig. 1 (Color online) (a) A schematic view of the optical pump and terahertz probe experiment in reflection geometry. (b)-(d) Temperature dependence of reflectivity, loss function, and real-part conductivity spectra at equilibrium (without pump).

Fig. 2 (Color online) (a) The waveform of the THz probe pulse. (b) Dynamics of the change of the probe THz electric field at its peak indicated by the dotted line in (a) as a function of t at 5 K. (c) and (d) Raw data of the transient reflectivity spectra for various pump intensities with a fixed t=100 ps and for various delays with a fixed intensity I_{pump}=3.6 mJ/cm^2, respectively.

Fig. 3 (Color online) (a)-(d) Transient reflectivity, loss function, real- and imaginary-part conductivity spectra of the photoexcited surface region, respectively in the weak excitation regime (I_{pump}<0.5 mJ/cm^2). The corresponding spectra in the strong excitation regime are shown in (e)-(h). (i)-(l) The calculated response functions obtained from the fits to the experimental results.

Fig. 4 (Color online) (a) Values of d_{pump} used in the analysis. Black circles are d_{pump}=600 nm and the green circles are evaluated in the strong excitation regime (see text). (b) The circles and squares show the peak energies observed in the loss function and conductivity spectra, respectively, as a function of the pump intensity. L indicates the original longitudinal mode. L' and T' denote the photoinduced longitudinal and transverse modes. The marker on the left axis shows the value in equilibrium. The dotted vertical line shows the energy required to suppress the superconductivity estimated from Ref. 30. (c) A schematic of the alternating Josephson coupling.

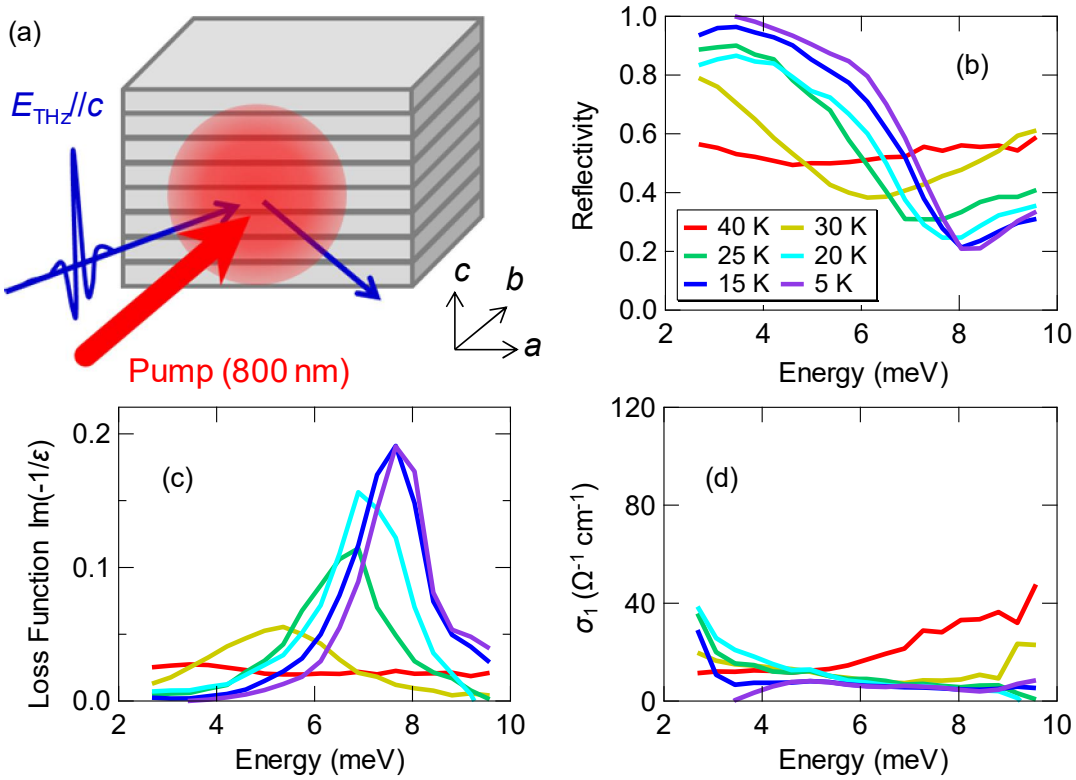
(a)
E_{THz}//c
c
b
a
Pump (800 nm)
(b)
Reflectivity
40 K
30 K
25 K
20 K
15 K
5 K
Energy (meV)
(c)
Loss Function Im(-1/ε)
Energy (meV)
(d)
σ_1 (Ω^{-1} cm^{-1})
Energy (meV)

Figure 1

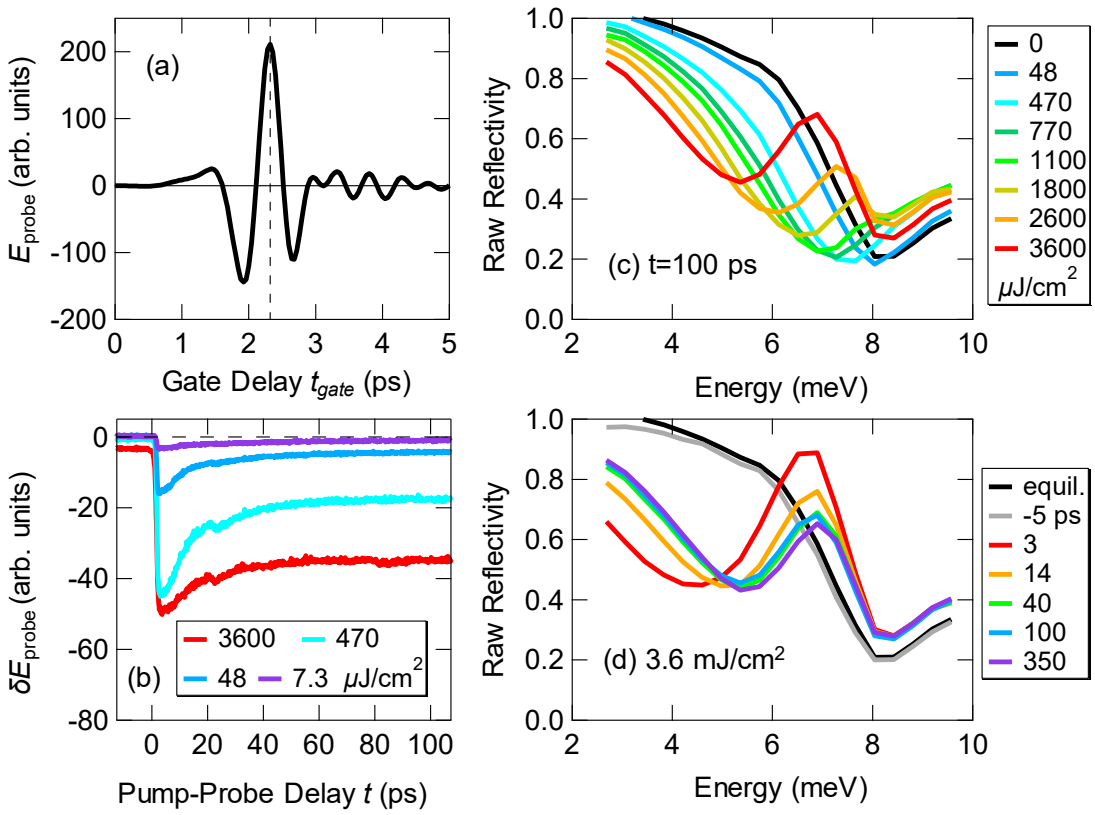
(a)
E_{probe} (arb. units)
Gate Delay t_{gate} (ps)
(b)
δE_{probe} (arb. units)
Pump-Probe Delay t (ps)
3600
470
48
7.3 μJ/cm^2
(c) t=100 ps
Raw Reflectivity
Energy (meV)
0
48
470
770
1100
1800
2600
3600
μJ/cm^2
(d) 3.6 mJ/cm^2
equil.
-5 ps
3
14
40
100
350

Figure 2

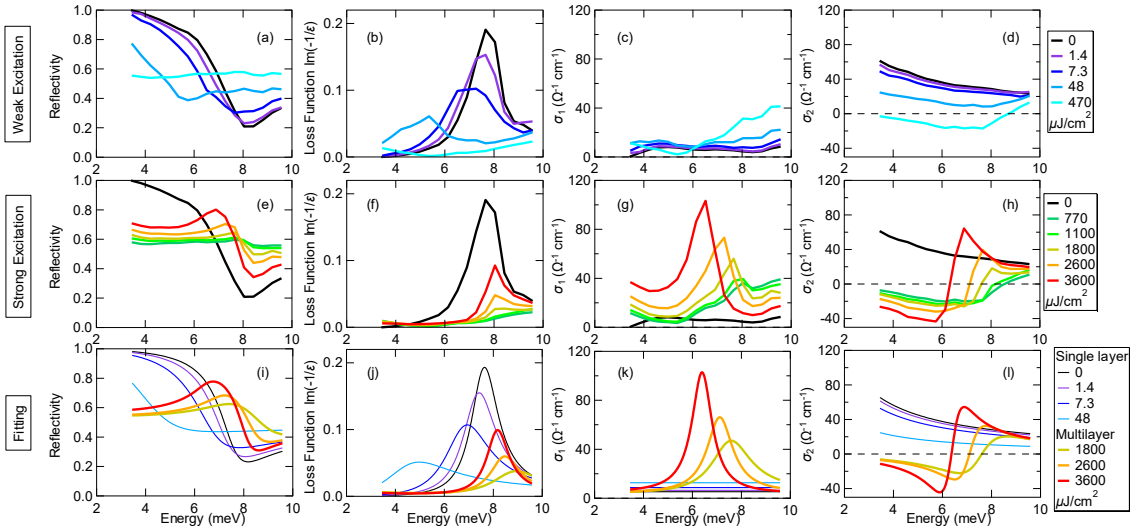
Weak Excitation
Strong Excitation
Fitting
Reflectivity
Loss Function Im(-1/ε)
σ1 (Ω-1 cm-1)
σ2 (Ω-1 cm-1)
Energy (meV)
(a)
(b)
(c)
(d)
(e)
(f)
(g)
(h)
(i)
(j)
(k)
(l)
0
1.4
7.3
48
470
μJ/cm2
0
770
1100
1800
2600
3600
μJ/cm2
Single layer
0
1.4
7.3
48
Multilayer
1800
2600
3600
μJ/cm2

Figure 3

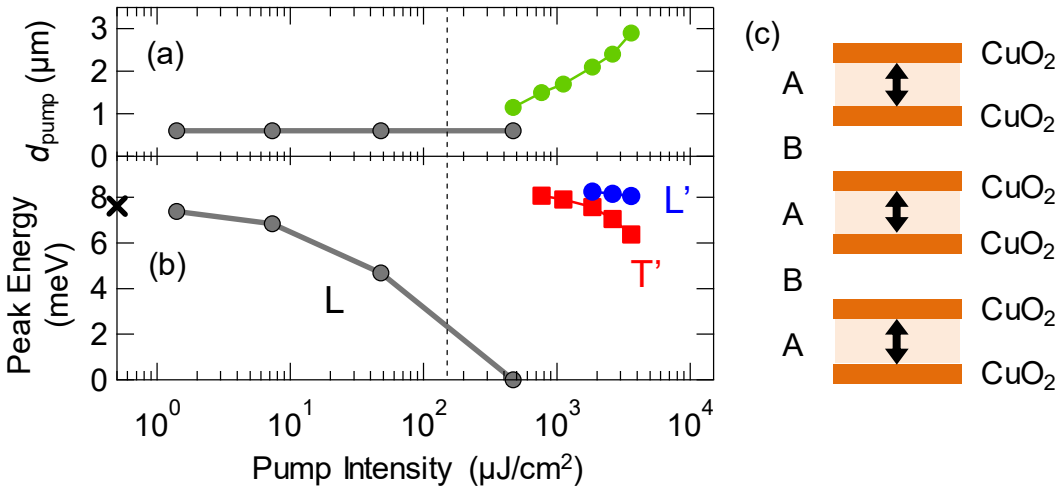
(a)
(b)
(c)
d_{pump} (μm)
Peak Energy (meV)
Pump Intensity (μJ/cm²)
L
L'
T'
A
B
A
B
A
CuO₂
CuO₂
CuO₂
CuO₂
CuO₂
CuO₂

Figure 4

References

[1] For a review, see *e.g.*, B. Keimer, S. A. Kivelson, M. R. Norman, S. Uchida, J. Zaanen, Nature **518**, 179 (2015)

[2] For a review, see *e.g.*, C. Giannetti, M. Capone, D. Fausti, M. Fabrizio, F. Parmigiani, and D. Mihailovic, Adv. Phys. **6**, 58 (2016).

[3] S. Dal Conte, C. Giannetti, G. Coslovich, F. Cliento, D. Bossini, T. Abebaw, F. Banfi, G. Ferrini, H. Eisaki, M. Greven, A. Damascelli, D. van der Marel, and F. Parmigiani, Science **335**, 1600 (2012)

[4] M. Sentef, A. F. Kemper, B. Moritz, J. K. Freericks, Z-X. Shen, and T. P. Devereaux, Phys. Rev. X **3**, 041033(2013).

[5] R. Matsunaga, Y. I. Hamada, K. Makise, Y. Uzawa, H. Terai, Z. Wang, and R. Shimano, Phys. Rev. Lett. **111**, 057002 (2013).

[6] R. Matsunaga, N. Tsuji, H. Fujita, A. Sugioka, K. Makise, Y. Uzawa, H. Terai, Z. Wang, H. Aoki, and R. Shimano, Science **345**, 1145 (2014).

[7] J. P. Hinton, J. D. Koralek, Y. M. Lu, A. Vishwanath, J. Orenstein, D. A. Bonn, W. N. Hardy, and Ruixing Liang, Phys. Rev. B **88**, 060508 (2013).

[8] G. L. Dakovski, W-S. Lee, D. G. Hawthorn, N. Garner, D. Bonn, W. Hardy, Ruixing Liang, M. C. Hoffmann, and J. J. Turner, Phys. Rev. B **91**, 220506 (2015).

[9] G. Yu, c. H. Lee, A. J. Heeger, N. Herron, E. McCarron, Lin Cong, G. C. Spalding, C. A. Nordman, and A. M. Goldman, Phys. Rev. B 45, 4964 (1992)

[10] S. Kaiser, C. R. Hunt, D. Nicoletti, W. Hu, I. Gierz, H. Y. Liu, M. Le Tacon, T. Loew, D. Haug, B. Keimer, and A. Cavalleri, Phys. Rev. B **89**, 184516 (2014).

[11] D. Fausti, R. I. Tobey, N. Dean, S. Kaiser, A. Dienst, M. C. Hoffmann, S. Pyon, T. Takayama, H. Takagi, and A. Cavalleri, Science **331**, 189 (2011).

[12] W. Hu, S. Kaiser, D. Nicoletti, C. R. Hunt, I. Gierz, M. C. Hoffmann, M. Le Tacon, T. Loew, B. Keimer, and A. Cavalleri, Nature Mater. **13**, 705 (2014).

[13] C. R. Hunt, D. Nicoletti, S. Kaiser, D. Pröpper, T. Loew, J. Porras, B. Keimer, and A. Cavalleri, Phys. Rev. B **94**, 224303 (2016).

[14] D. Nicoletti, E. Casandruc, Y. Laplace, V. Khanna, C. R. Hunt, S. Kaiser, S. S. Dhesi, G. D. Gu, J. P. Hill, and A. Cavalleri, A. Phys. Rev. B **90**, 100503 (2014).

[15] K. Tamasaku, Y. Nakamura, and S. Uchida, Phys. Rev. Lett. **69**, 1455 (1992).

[16] S. Uchida, K. Tamasaku, and S. Tajima, Phys. Rev. B **53**, 14558 (1996).

[17] S. V. Dordevic, S. Komiya, Y. Ando, and D. N. Basov, Phys. Rev. Lett. **91**,

167401 (2003).
[18] For a review, see *e.g.*, S. Tajima and S. Uchida, Physica C **481**, 55 (2012).
[19] See Supplemental Material for details of the calculation.
[20] P. Kusar, V. V. Kabanov, J. Demsar, T. Mertelj, S. Sugai, and D. Mihailovic, Phys. Rev. Lett. **101**, 227001 (2008).
[21] M. Beyer, D. Städter, M. Beck, H. Schäfer, V. V. Kabanov, G. Logvenov, I. Bozovic, G. Koren, J. Demsar, Phys. Rev. B **83**, 214515 (2011).
[22] H. Shibata and T. Yamada, Phys. Rev. Lett. **81**, 3519 (1998).
[23] T. Kakeshita, S. Uchida, K. M. Kojima, S. Adachi, S. Tajima, B. Gorshunov, and M. Dressel, Phys. Rev. Lett. **86**, 4140 (2001).
[24] D. Dulić, A. Pimenov, D. van der Marel, D. M. Broun, S. Kamal, W. N. Hardy, A. A. Tsvetkov, I. M. Sutjaha, R. Liang, A. A. Menovsky, A. Loidl, S. S. Saxena, Phys. Rev. Lett. **86**, 4144 (2001).
[25] H. Shibata, Phys. Rev. Lett. **86**, 2122 (2001).
[26] M. Grüninger, D. van der Marel, A. A. Tsvetkov, and A. Erb, Phys. Rev. Lett. **84**, 1575 (2000).
[27] V. Železný, S. Tajima, D. Munzar, T. Motohashi, J. Shimoyama, and K. Kishio, Phys. Rev. B **63**, 060502 (2001).
[28] K. M. Kojima, S. Uchida, Y. Fudamoto, and S. Tajima, Phys. Rev. Lett. **89**, 247001 (2002).
[29] L. Bulaevskii and J. R. Clem, Phys. Rev. B **44**, 10234 (1991).
[30] D. van der Marel and A. Tsvetkov, Czech. J. Phys. **46**, 3165 (1996).
[31] D. van der Marel and A. A. Tsvetkov, Phys. Rev. B **64**, 024530 (2001).
[32] A. Dubroka, M. Rössle, K. W. Kim, V. K. Malik, D. Munzar, D. N. Basov, A. A. Schafgans, S. J. Moon, C. T. Lin, D. Haug, V. Hinkov, B. Keimer, Th. Wolf, J. G. Storey, J. L. Tallon, and C. Bernhard, Phys. Rev. Lett. **106**, 047006 (2011).
[33] N. Gedik, D.-S. Yang, G. Logvenov, I. Bozovic, and A. H. Zewail, Science **316**, 425 (2007).
[34] P. Kusar, V.V. Kabanov, S. Sugai, J. Demsar, T. Mertelj, D. Mihailovic, J. Supercond. Nov. Magn. **24**, 241 (2011).
[35] J. H. Kim, H. S. Somal, M. T. Czyzyk, D. van der Marel. A. Wittlin, A. M. Gerrits, V. H. M. Duijn, N. T. Hien, and A. A. Menovsky, Physica C **247**, 297 (1995).
[36] D. N. Basov, H. A. Mook, B. Dabrowski, and T. Timusk, Phys. Rev. B **52**, R13141 (1995).
[37] T. Matsuoka, T. Fujimoto, K. Tanaka, S. Miyasaka, S. Tajima, K. Fujii, M.

Suzuki, and M. Tonouchi, Physica C **469**, 982 (2009).

Supplemental Material for

Light-induced switching to a Metastable Phase in a Layered Superconductor $La_{2-x}Sr_xCuO_4$ (x=0.15)

Kaito Tomari, Ryusuke Matsunaga, Hiroaki Niwa, Dongjoon Song, Hiroshi Eisaki, and Ryo Shimano

Temperature dependence of the transient reflectivity spectra

We performed the pump-probe experiments in the optimally-doped LSCO at various temperatures. Figures S1(a)-(d) show the transient reflectivity spectra at 20 K, 25 K, 30 K, and 40 K for various excitation intensities. The additional reflectivity edge discussed in the main text was observed at any temperature below T_c=35.5 K for sufficiently strong excitation densities. At 40 K above T_c, however, the reflectivity simply decreases upon the photoexcitation for all the frequency range (~2-9 meV) without showing any peak even for the strongest excitation beyond 3 mJ/cm^2. The results clearly indicate that the newly developed reflectivity edge at strong photoexcitations originates from the Josephson coupling between the CuO_2 planes.

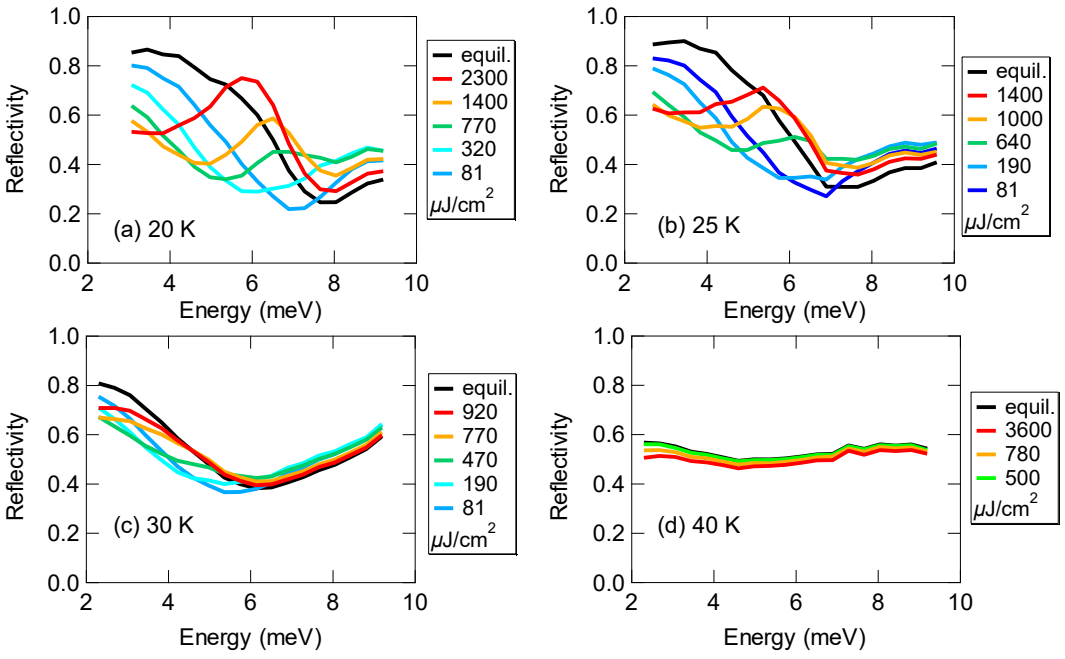

Fig. S1 Transient reflectivity spectra and at (a) 20 K, (b) 25 K, (c) 30 K and (d) 40 K at the delay time of t=3 ps. The black curves show the spectra in equilibrium without pump.

Transient reflectivity spectra with photoexcitation polarized along the *a*-axis

The solid curves and broken curve in Fig. S2 show the results of the pump-probe experiments with the polarization of the optical pump pulse parallel to the *a* and *c* axes, respectively. At the strong excitation above 1 mJ/cm^2 polarized along the *a* axis, the additional plasma edge was also observed as similar to the case of the *c*-axis polarization. The results indicate that the metastable phase can be induced irrespective to the pump polarization direction within the *ac* surface.

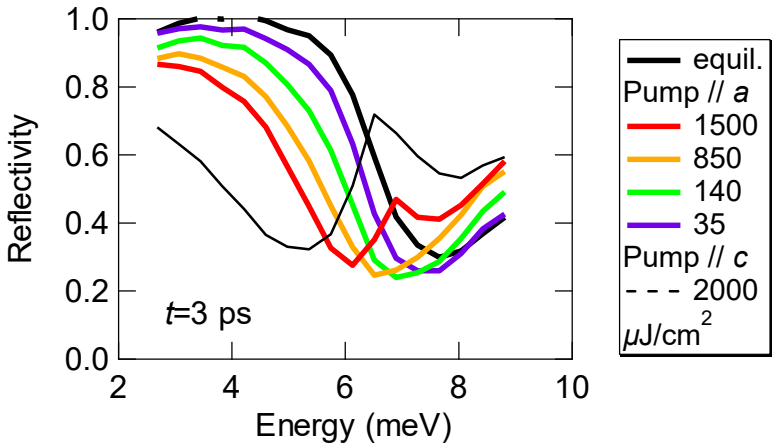

Fig. S2 Transient reflectivity spectra at 5 K and *t*=3 ps. The solid curves and broken curve show the results of the optical pump polarized along the *a* and *c* axis, respectively.

Analysis of the transient response function of the photoexcited surface regions

i) Penetration depth mismatch

From the real-part optical conductivity of 100 Ω^{-1}cm^{-1} and the reflectivity of 0.15 at 800 nm in the optimally-doped LSCO for the *c* axis polarization [S1], the real-part dielectric function is estimated to be 5.1 and then the penetration depth of the optical pump pulse to be 600 nm in equilibrium. Since the penetration depth of the probe THz wave is much larger than that of the optical pump pulse, we use the following phenomenological model considering a series of photoexcited thin layers at the distance *z* from the surface as shown in Fig. S3 [S2, S3].

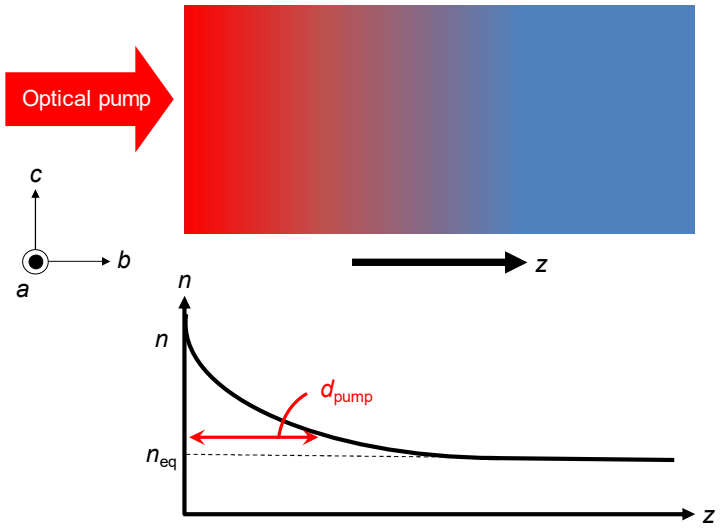

Fig. S3 A schematic of the photoexcitation from the *ac* surface (left side). The lower panel shows the *z*-dependent refractive index described in Eq. (S6).

Assuming an exponential decay profile for the effect of the photoexcitation on the complex refractivity, we described the refractive index of a layer with distance z as

$$n(\omega,z)=n_{eq}(\omega)+\left[n(\omega)-n_{eq}(\omega)\right]\exp\left(-z/d_{pump}\right), \tag{S6}$$

where $n(\omega)=\sqrt{\varepsilon(\omega)}$ and $n_{eq}(\omega)=\sqrt{\varepsilon_{eq}(\omega)}$ are the refractive indices of the photoexcited surface and in equilibrium, respectively. We consider the depth L=20 μm from the *ac* surface and divide it into N=1000 layers. When we consider only the deepest Nth layer on the backside bulk LSCO as shown in Fig. S4(a), the incident wave acquires an effective Fresnel coefficient which includes the effect of the Nth layer and the unperturbed LSCO as

$$\begin{aligned}\tilde{r}_N &= r_{N-1,N}+\frac{t_{N-1,N}r_{N,bulk}t_{N,N-1}e^{i2\frac{n\omega}{c}\frac{L}{N}}}{1-r_{N,N-1}r_{N,bulk}e^{i2\frac{n\omega}{c}\frac{L}{N}}} \\ &= \frac{r_{N-1,N}+r_{N,bulk}e^{i2\frac{n\omega}{c}\frac{L}{N}}}{1+r_{N-1,N}r_{N,bulk}e^{i2\frac{n\omega}{c}\frac{L}{N}}},\end{aligned} \tag{S7}$$

where

$$t_{m,m+1} = \frac{2n(\omega, mL/N)}{n(\omega, mL/N) + n(\omega, (m+1)L/N)},$$
$$r_{m,m+1} = \frac{n(\omega, mL/N) - n(\omega, (m+1)L/N)}{n(\omega, mL/N) + n(\omega, (m+1)L/N)}, \quad \text{(S8)}$$

are the Fresnel coefficients for transmittance and reflection at the boundary between mth and (m+1)th layers (m=1,2,…N). Here $n(\omega, mL/N)$ is the refractive index of mth layer obtained from Eq. (S6), and

$$r_{N,bulk} = \frac{n(\omega, L) - n_{eq}(\omega)}{n(\omega, L) + n_{eq}(\omega)}, \quad \text{(S9)}$$

is the Fresnel coefficient at the boundary between the Nth layer and the backside bulk in equilibrium. Similarly, by using $\tilde{r}_N$ in Eq. (S7), the effective Fresnel coefficient for the (N-1)th, Nth layers, and the bulk LSCO can expressed as

$$\tilde{r}_{N-1,N} = \frac{r_{N-2,N-1} + \tilde{r}_N e^{i2\frac{n\omega}{c}\frac{L}{N}}}{1 + r_{N-2,N-1}\tilde{r}_N e^{i2\frac{n\omega}{c}\frac{L}{N}}}, \quad \text{(S10)}$$

as shown in Fig. S4(b). Repeating this calculation, we obtained the total effective Fresnel coefficient $\tilde{r}_{1,2,\ldots,N-1,N}$. Then we define the total effective refractive index $n^{eff}(\omega)$ as

$$n^{eff}(\omega) \equiv \frac{1 - \tilde{r}_{1,2,\ldots,N-1,N}(\omega)}{1 + \tilde{r}_{1,2,\ldots,N-1,N}(\omega)}. \quad \text{(S11)}$$

The raw data of the experimentally-observed energy reflectivity $R^{eff}(\omega)$ in Figs. 2(c) and 3(a) is related with the effective refractive index as

$$R^{eff}(\omega) = \left| \frac{1 - n^{eff}(\omega)}{1 + n^{eff}(\omega)} \right|^2. \quad \text{(S12)}$$

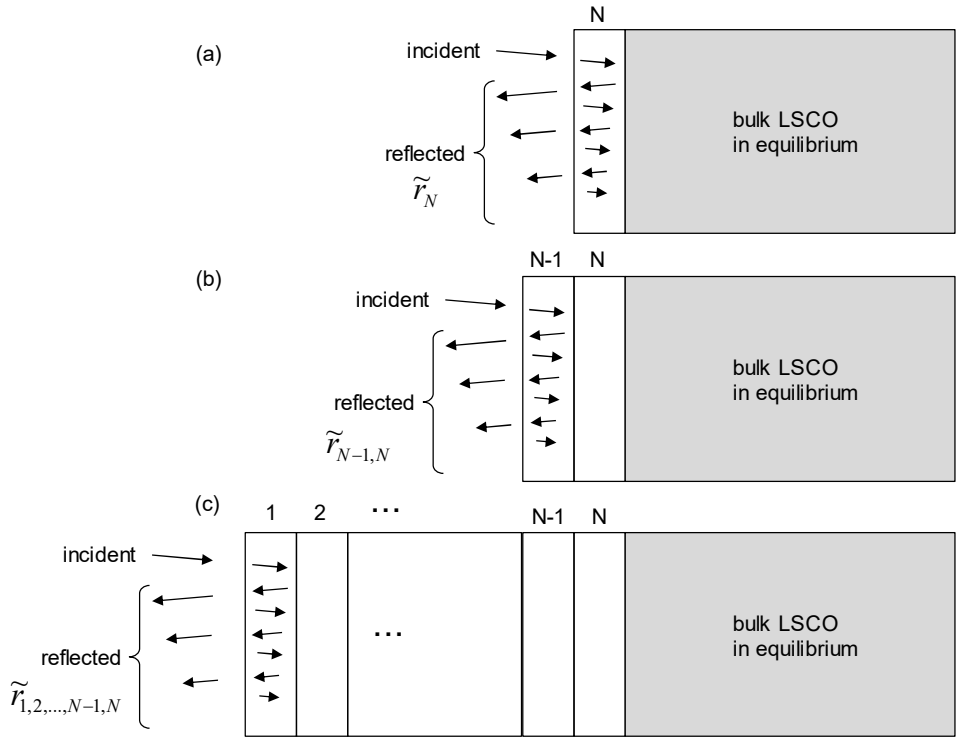

Fig. S4 The reflection from the photoexcited N layers on top of the unperturbed bulk LSCO.

ii) Evaluation of d_{pump}

From the above analysis, as far as d_{pump} is given, the dielectric function of the photoexcited surface $\varepsilon(\omega)=\varepsilon_1(\omega)+i\varepsilon_2(\omega)=n(\omega)^2$ can be extracted from the measured reflectivity $R^{eff}(\omega)$ and its phase information which were obtained by the THz time-domain spectroscopy.

For the weak excitation regime below 0.5 mJ/cm^2, we fixed the value of d_{pump} to 600 nm, the penetration depth of the 800-nm optical pump. The obtained transient response functions with various photoexcitation intensities are shown in Figs. 2(c)-2(f), which can be reasonably understood by the light-induced suppression of superconductivity as discussed in the main text.

For stronger excitation regime, however, we have to determine d_{pump} as a pump intensity-dependent value because the effect of the strong photoexcitation penetrates into the bulk LSCO much more deeply than 600 nm. In fact, d_{pump} defined in Eq. (S6) is not a penetration depth of the optical pulse at 800 nm but rather represents the length scale at which the photoexcitation modifies the refractive index of the bulk LSCO from its equilibrium value. Having seen that the refractive index is significantly altered already at I_{pump}=48 μJ/cm^2 as shown in Figs. 3(a)-3(d), d_{pump} should be extended much

longer than 600 nm in the case of much stronger photoexcitation.

To determine d_{pump}, here we focused on the value of $\sigma_2(\omega)$ at the dc limit since it must be 0 in a normal state or diverge in a superconducting state. As described in the main text, we set d_{pump} so that $\sigma_2(\omega)$ asymptotically approaches to 0 at in the dc limit. The obtained response functions of the surface regions and the values of d_{pump} used in the analysis are shown in Figs. 3(e)-3(h) and Fig. 4(a), respectively. The validity for the value of d_{pump} is further examined in the next section.

iii) Examination of d_{pump} used in the analysis

To examine the validity of d_{pump} used in the analysis above, we evaluated the photoexcitation densities at $z=d_{pump}$ from the surface, which are plotted by the red circles in Fig. S5. The values stay within the range of values ~30-70 μJ/cm^2. Compared with Fig. 2(d), these values are reasonably strong to induce the substantial change of the refractive index, which confirms that the values of d_{pump} used in the analysis are consistent.

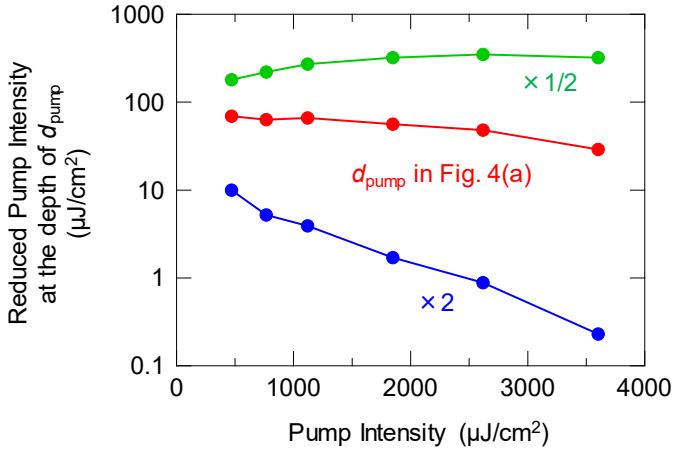

Fig. S5 The pump intensity at the depth of $z=d_{pump}$ from the surface. The red circles show the case of d_{pump} used in the analysis. The green and blue circles correspond to the cases of d_{pump} multiplied by 1/2 and 2, respectively.

Here we also check how the response functions could be altered if we change the value of d_{pump} in the analysis. We compare the reduced excitation densities at the depth of $z=d_{pump}$ in Fig. S5 where d_{pump} is factored by 1/2 or 2. We also calculated the response functions in Fig. S6. If we multiply d_{pump} by 1/2 (the green circles in Fig. S5 and the left panels in Fig. S6), $\sigma_2(\omega)$ approaches to a negative value in the dc limit, which is indeed unphysical, and the reflectivity is unnaturally high. If d_{pump} is factored

by 2 (the blue circles in Fig. S5 and the right panels in Fig. S6), the reduced photoexcitaton densities at the depth of $z=d_{pump}$ become too small to modify the refractive index. Therefore, the trial values of d_{pump} in these two cases are apparently too small or too large. Nevertheless, the difference of d_{pump} does not substantially alter the essential spectral features of the response functions as represented in Fig. S6. From this consideration, we can conclude that the obtained response functions in Fig. 3 are less sensitive to the way of analysis and reliable enough to discuss the underlying physics induced by the strong photoexcitation.

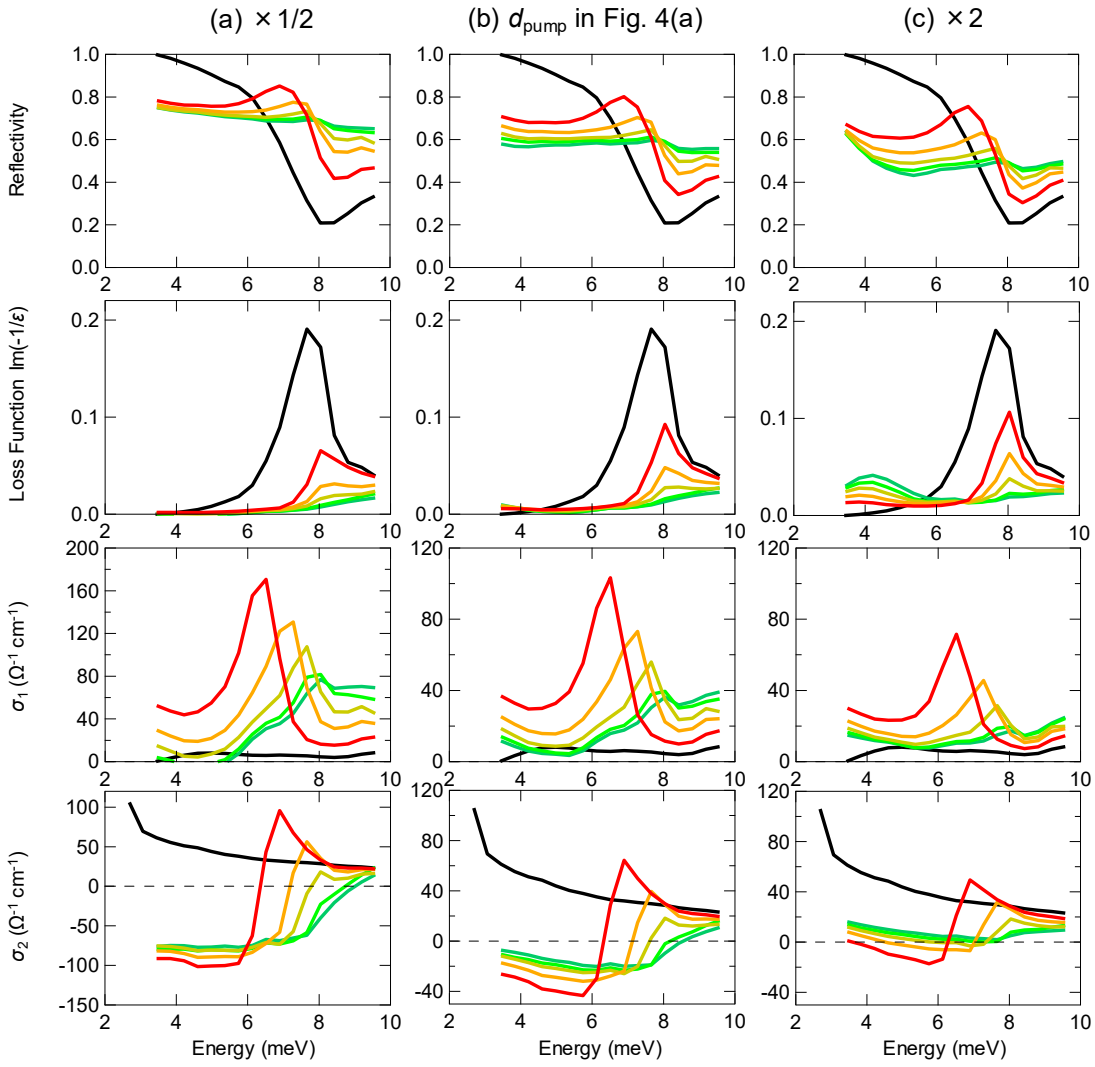

Fig. S6 Response functions obtained from different settings of d_{pump}. The middle panels (b) show the response functions of the photoexcited surface with d_{pump} we used in the main text, *i.e.*, equivalent to Fig. 3. The left (a) and right (c) panels show the cases of d_{pump} factored by 1/2 and 2, respectively.

Multilayer model

If the superconductivity is locally collapsed in a random manner upon the photoexcitation, the randomness of the coupling energies would broaden the loss function peak [S5], which contradicts the experimental observation that a well-defined sharp mode appears in the higher energy side. Therefore, it is reasonable to interpret that alternating two distinct Josephson junctions are induced under the strong photoexcitation. We adopt the multilayer model to describe such asymmetric Josephson couplings in the stacked layer system [S6, S7].

The local couplings at the junctions A and B are written in the two-fluid model as

$$\varepsilon_j(\omega) = \varepsilon_\infty\left[1-\frac{\omega_j^2}{\omega^2}+i\frac{\Gamma_j}{\omega}\right], \quad (j\text{=A, B}) \tag{S1}$$

where ω_j is the local coupling energy at the junction j and Γ_j is the scattering rate originating from normal fluid components. The total dielectric functions in the multilayer model are then written as

$$\frac{1}{\varepsilon_{\mathrm{MLM}}(\omega)} = \sum_j \frac{z_j}{\varepsilon_j(\omega)}, \tag{S2}$$

where z_j are the weight factors for the junction j and $\sum_j z_j = 1$. If we ignore the scattering term Γ_j for simplicity, Eq. (S2) gives

$$\varepsilon_{\mathrm{MLM}}(\omega) = \varepsilon_\infty \frac{\left(\omega^2-\omega_A^2\right)\left(\omega^2-\omega_B^2\right)}{\omega^2\left(\omega^2-\omega_T^2\right)}, \tag{S3}$$

where $\omega_T \equiv \sqrt{z_A\omega_B^2 + z_B\omega_A^2}$ is the transverse plasma mode frequency. In the extended multilayer model [S7], Eq. (S2) is modified as

$$\frac{1}{\varepsilon_{\mathrm{MLM}}(\omega)} = \sum_j \frac{\tilde{z}_j}{\varepsilon_\infty\left[1-\frac{\tilde{\omega}_j^2}{\omega^2}+i\frac{\Gamma_j}{\omega}\right]}, \tag{S4}$$

where

$$\tilde{\omega}_A^2 \equiv \left(\frac{1}{2}+\frac{\gamma}{z_A}\right)\omega_A^2 + \left(\frac{1}{2}+\frac{\gamma}{z_B}\right)\omega_B^2 - \sqrt{\left[\left(\frac{1}{2}+\frac{\gamma}{z_A}\right)\omega_A^2 - \left(\frac{1}{2}+\frac{\gamma}{z_B}\right)\omega_B^2\right]^2 + \frac{\left(2\gamma\omega_A\omega_B\right)^2}{z_A z_B}},$$

$$\widetilde{\omega}_B^2 \equiv \left(\frac{1}{2}+\frac{\gamma}{z_A}\right)\omega_A^2+\left(\frac{1}{2}+\frac{\gamma}{z_B}\right)\omega_B^2+\sqrt{\left[\left(\frac{1}{2}+\frac{\gamma}{z_A}\right)\omega_A^2-\left(\frac{1}{2}+\frac{\gamma}{z_B}\right)\omega_B^2\right]^2+\frac{(2\gamma\omega_A\omega_B)^2}{z_A z_B}},$$

$$\widetilde{z}_A \equiv 1-\widetilde{z}_B \equiv \frac{1}{2}-\frac{(z_B-z_A)(\omega_B^2-\omega_A^2)-2\gamma(\omega_B^2/z_B+\omega_A^2/z_A)}{2\sqrt{\left[(1+2\gamma/z_B)\omega_B^2-(1+2\gamma/z_A)\omega_A^2\right]^2+4(2\gamma\omega_A\omega_B)^2/z_A z_B}}.$$

Here γ is proportional to the inverse of the electron compressibility which was introduced to account for the plasma dispersion [S7].

The thick curves in Figs. 3(i)-3(l) are the results of the simulation, which well reproduces the experimental results in Figs. 3(d)-3(h). Here we fixed the parameters of z_A=z_B=0.5, ω_B=0 meV, and Γ_B=0.83 meV. The other parameters used in the calculation are summarized in Fig. S7. We also performed the fitting to the experimental data in the weak excitation regime below 48 μJ/cm^2 by using a single layer model. The results are also shown as thin curves in Figs. 3(i)-3(l).

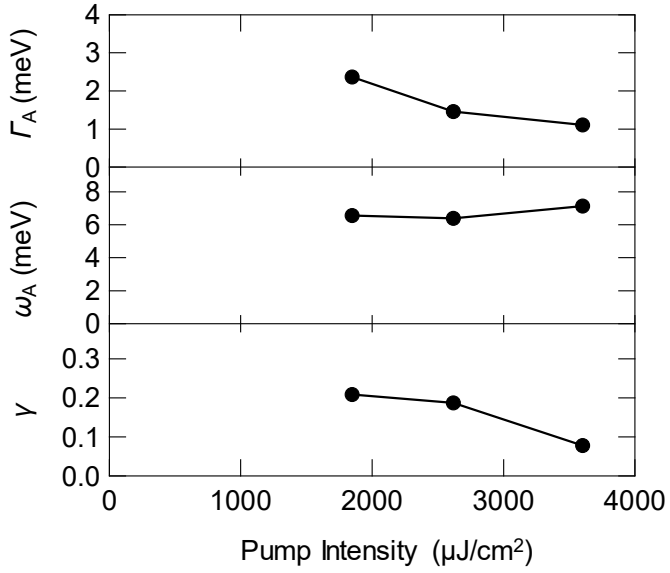

Fig. S7 The parameters of the multilayer model used in the fitting in Fig. 3.

As I_{pump} increases, the coupling energy at the junction A slightly increases with decreasing scattering rate, which indicates the growth of Josephson coupling at the junction A for such a strong excitation regime. For the intermediate excitation intensities of 470-1100 μJ/cm^2, the multilayer model does not well reproduce the experimental curves. One reason is the broad absorption band around 10 meV which becomes most prominent in the $\sigma_1(\omega)$ spectra at intermediate excitation densities as shown in Figs. 3(c) in the main text. The photoinduced transverse JPR mode seems distinct from this broad

absorption band since it starts to appear around 1100 μJ/cm^2 as a tiny peak on top of this broad absorption band with a much sharper resonance width. To properly fit the spectrum in the intermediate excitation density region, another model function including this broad absorption effect is needed. Another remarkable feature is the reduction of γ, which is required to reproduce the shift of the transverse mode energy with holding the longitudinal mode energy almost intact. The reduction of γ corresponds to the increase of electron compressibility in the extended multilayer model [S7] and details of the pump intensity dependence are left to be clarified in future work.

References

[S1] S. Uchida, K. Tamasaku, and S. Tajima, Phys. Rev. B **53**, 14558 (1996).

[S2] S. Kaiser, C. R. Hunt, D. Nicoletti, W. Hu, I. Gierz, H. Y. Liu, M. Le Tacon, T. Loew, D. Haug, B. Keimer, and A. Cavalleri, Phys. Rev. B **89**, 184516 (2014).

[S3] C. R. Hunt, D. Nicoletti, S. Kaiser, D. Pröpper, T. Loew, J. Porras, B. Keimer, and A. Cavalleri, Phys. Rev. B **94**, 224303 (2016).

[S4] P. Kusar, V. V. Kabanov, J. Demsar, T. Mertelj, S. Sugai, and D. Mihailovic, Phys. Rev. Lett. **101**, 227001 (2008).

[S5] M. Beyer, D. Städter, M. Beck, H. Schäfer, V. V. Kabanov, G. Logvenov, I. Bozovic, G. Koren, J. Demsar, Phys. Rev. B **83**, 214515 (2011).

[S6] S. V. Dordevic, S. Komiya, Y. Ando, and D. N. Basov, Phys. Rev. Lett. **91**, 167401 (2003).

[S7] D. van der Marel and A. Tsvetkov, Czech. J. Phys. **46**, 3165 (1996).

[S8] D. van der Marel and A. A. Tsvetkov, Phys. Rev. B **64**, 024530 (2001).